V. MICROWAVE ELECTRONICS

Prof. L. D. Smullin   P. Chorney[†]   S. Holly
Prof. H. A. Haus   H. W. Fock[†]   A. Saharian
A. Bers   T. J. Goblick, Jr.   A. Zacharias

A. MODE COUPLING IN PERIODIC STRUCTURES BY VARIATIONAL TECHNIQUES

A periodic slow-wave structure with heavy shunt loading has been treated by R. M. Bevensee from a mode-coupling approach (1, 2). With heavy shunt loading the coupling between adjacent sections of the structure is weak, and the structure resembles a chain of coupled resonant cavities. In the mode-coupling approach, the fields of the structure were approximated by resonant cavity modes of a section of the structure. This approach led to coupling equations that relate the angular frequency, ω, to the phase shift per section, ϕ. The validity of this approach was checked by comparing curves of ω^2 versus ϕ for a transmission line that is periodically shunted with capacitors (3, 4).

With the mode-coupling formalism for analyzing a periodic structure, only a finite number of terms can be handled mathematically in approximating the fields of the structure. It is not clear from the mode-coupling formalism why these simplifications can be made and accurate results still obtained. The mathematical technique that allows the use of approximate functions for calculating certain characteristic values in boundary-value problems, and yields the best possible answers, involves the use of the variational calculus. A variational principle relating frequency and phase shift per section for periodic structures was obtained, and by using appropriate trial fields the approximate propagation characteristics could then be calculated. With a heavily loaded periodic structure, the trial fields that were chosen were normal cavity modes of a section of the structure. It is interesting to note that the same mode-coupling equations that were found by Bevensee (1) are also obtained by using this variational principle.

In a periodic structure the electric field $\overline{E}_+(u_1, u_2, z)$ satisfies the wave equation

$$\nabla \times \nabla \times \overline{E}_+ - k^2\overline{E}_+ = 0 \qquad\qquad k^2 = \omega^2 \mu \epsilon \qquad\qquad (1)$$

when the medium filling the structure is isotropic and homogeneous (u_1 and u_2 are generalized transverse coordinates). The boundary condition

$$\overline{n} \times \overline{E}_+ = 0 \quad \text{on } S \qquad\qquad (2)$$

is also satisfied, where $\overline{n}$ is the unit vector normal to the perfectly conducting walls S. Another important property of the fields of a periodic structure comes from Floquet's theorem.

[†] From Raytheon Manufacturing Company.

$$\overline{E}_+(u_1, u_2, z + L) = \overline{E}_+(u_1, u_2, z)\, e^{-j\phi} \tag{3}$$

where L is the length of one period of the structure, and the direction of propagation is in the positive z-direction.

If Eq. 1 is dot-multiplied by an adjoint wave solution $\overline{E}_-^*$, and an integration throughout the volume V of one cavity section is performed, the result is the variational principle for k^2:

$$k^2 = \frac{\displaystyle\int_V \overline{E}_-^* \cdot \nabla \times \nabla \times \overline{E}_+ \, dv}{\displaystyle\int_V \overline{E}_-^* \cdot \overline{E}_+ \, dv} \tag{4}$$

Knowing the exact $\overline{E}_+$ field would enable us to calculate the value of k^2, but since we do not know the exact field, approximate (trial) fields are used for $\overline{E}_+$ and $\overline{E}_-$ to find approximate values of k^2. For certain restrictions on these trial fields we can show that the first-order variation of k^2 vanishes; that is

$$\delta [k^2] = 0 \tag{5}$$

which shows that Eq. 3 is a variational principle. These restrictions on the adjoint solution and the trial fields, denoted by $\overline{E}_+^T$ and $\overline{E}_-^T$, are:

(a) $\nabla \times \nabla \times \overline{E}_-^* - k^2 \overline{E}_-^* = 0$ is satisfied by the adjoint solution.

(b) $\bar{n} \times \overline{E}_-^* = 0$ on S is satisfied by the adjoint solution.

(c) The adjoint solution satisfies Floquet's theorem; that is $\overline{E}_-(u_1, u_2, z + L) = \overline{E}_-(u_1, u_2, z)\, e^{-j\phi}$.

(d) The first-order variation of the tangential component of the E_+ trial field must vanish on S: $\bar{n} \times \delta \overline{E}_+ = 0$ on S.

From conditions a, b, and c, the adjoint solution is recognized as a wave propagating along the periodic structure in the positive z-direction. An $\overline{E}_+^T$ trial field in a cavity section consistent with condition d was constructed as a linear superposition of "short-circuit modes" of a cavity section. (A short-circuit mode has no tangential component of electric field at the surfaces of the coupling holes. The holes have been effectively "short-circuited.") For the $\overline{E}_+^T$ trial field in adjacent sections, the same linear superposition was used except for a phase shift ϕ with respect to the trial field in the preceding cavity section so that Eq. 3 would be satisfied by $\overline{E}_+^T$. For the $\overline{E}_-^T$ trial field, a linear superposition of open-circuit modes of a cavity section was used, together with the same phase shift ϕ between fields of adjacent sections. (An open-circuit mode has no tangential magnetic-field component at the surfaces of the holes.)

For this assumed value of ϕ, an optimum value of k^2 can be calculated by using the variational principle of Eq. 4. The trial fields are discontinuous at the surfaces

of the coupling holes because of the phase shift between trial fields of adjacent sections, and this discontinuity leads to a surface integral over the area of the holes which involves a function of ϕ.

If the fields of the periodic structure are approximated in a certain frequency range by a single short-circuit resonant mode ($\overline{E}_+^T$ trial field) and a single open-circuit mode ($\overline{E}_-^T$ trial field), we obtain a very simple coupling equation which gives the k^2 versus ϕ characteristic as

$$k^2 = \left(\frac{P^2 + p^2}{2}\right) \mp \left(\frac{p^2 - P^2}{2}\right) \cos \phi \qquad (6)$$

$$P^2 = \omega_{sc}^2 \mu\epsilon \qquad p^2 = \omega_{oc}^2 \mu\epsilon$$

where ω_{sc} and ω_{oc} are the resonant angular frequencies of the short-circuit and open-circuit modes that are used. The minus sign of the $\mp$ combination is used for symmetrical trial fields; the plus sign is used for antisymmetrical trial fields.

This development shows that the formalism of mode coupling, which is intuitively appealing, has the variational principle as its mathematical foundation. The approximations in the choice of trial fields are made in such a way that the value of k^2 is minimized, and this is the reason for the accurate results obtained in many cases with greatly simplified trial fields.

T. J. Goblick, Jr.

References

1. R. M. Bevensee, Coupling-of-modes theory of periodic, lossless, electromagnetic cavity chains, E.E. Thesis, Department of Electrical Engineering, M.I.T., February 1958.

2. R. M. Bevensee, Mode coupling in periodic cavity chains, Quarterly Progress Report, Research Laboratory of Electronics, M.I.T., Oct. 15, 1957, p. 25.

3. T. J. Goblick, Jr., A study of mode coupling in periodic structures, E.E. Thesis, Department of Electrical Engineering, M.I.T., Jan. 1958.

4. T. J. Goblick, Jr., Mode coupling in a periodically loaded transmission line, Quarterly Progress Report, Research Laboratory of Electronics, M.I.T., Jan. 15, 1958, p. 50.

B. MICROWAVE BEAM MEASUREMENTS

1. Vacuum System

Low-noise beam measurements are hard to make in demountable systems because it is difficult to prevent poisoning of the very small cathodes that are commonly used. One of the annoying sources of trouble is back-diffusion of pump oil into the vacuum

system and onto the cathode. The back-diffusion of oil can be limited by improving the baffling or by using mercury pumps. We chose the former solution because of the increased pumping speed of the oil pump.

A mechanically refrigerated baffle is interposed between the oil-diffusion pump (MCF-400) and the liquid-nitrogen trap. Figure V-1 shows the major features of the cooled baffle, and Fig. V-2 shows the entire vacuum system.

Cooling of the baffle is accomplished by using a compressor and condenser from a used household refrigerator. The Freon-12 charge was removed and replaced by Freon-22. From a heat-loss calculation it was predicted that the capacity of the refrigeration system was approximately 50 times greater than that required for the baffle. We used the excess capacity to cool the outside wall of the liquid-nitrogen trap and thus retarded evaporation of the liquid nitrogen.

Because the compressor is limited (by age and design characteristics) to operation at a minimum suction pressure of zero psi (gauge), the lowest temperature obtainable with Freon-22 is -40° C, which is the boiling point of Freon-22 at one atmosphere. The use of a compressor that would operate at vacuum on the suction side would allow much lower temperatures to be obtained with a unit of the same capacity.

The vacuum system was operated at 6×10^{-6} mm Hg by the fore-pump and ejector pump, without either liquid-nitrogen or Freon cooling. When the refrigerated baffle was cooled to equilibrium temperature, the pressure was reduced to 2.5×10^{-6} mm Hg. Pressures were measured with a Bayard-Alpert gauge at
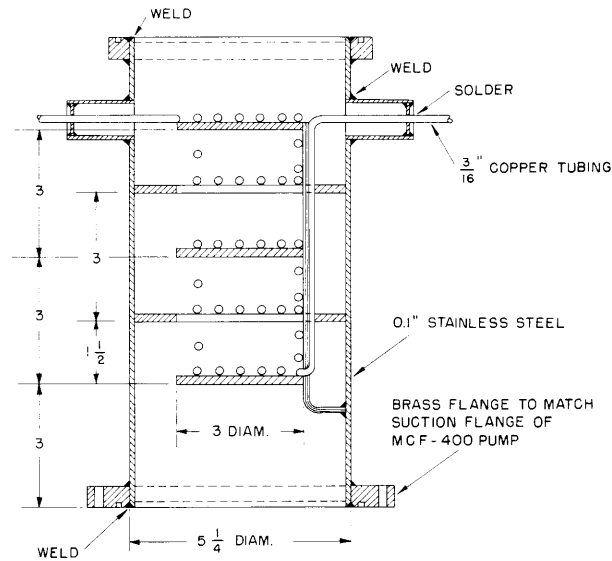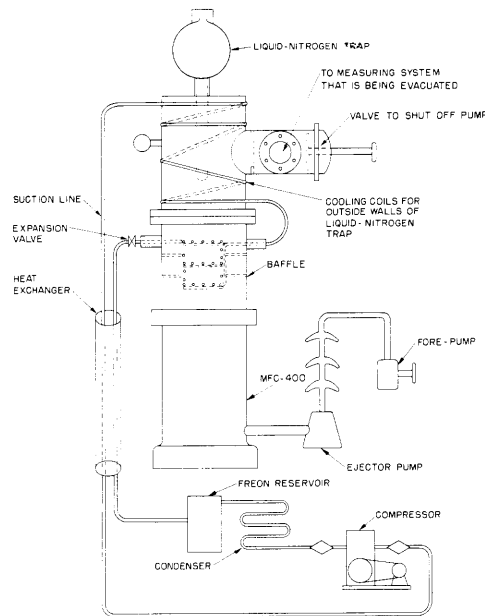

Fig. V-1. Refrigerated baffle.

Fig. V-2. Vacuum system.

point "A" in Fig. V-2. Operation of the MCF-400 diffusion pump reduced the pressure to approximately 5×10^{-7} mm Hg after a stabilization period of approximately 10 hours. The admission of liquid nitrogen into the trap further reduced the pressure to 2×10^{-7} mm Hg. The rate of evaporation of the liquid nitrogen depended on the quantity in the trap. This variation occurs because cooling to below $-20°$ C is accomplished on the outside walls of only that part of the trap which extends into the vacuum system. The large reservoir bowl does not have the outside walls cooled, and only the glass insulation can be depended upon for conductive isolation, and the silvered inside and outside walls for radiative isolation. The evaporation rate from the part extending into the vacuum system is approximately 1 pound per day, and from the reservoir bowl it is from 1.5 to 2.5 pounds per day. The full capacity is 7 pounds of liquid nitrogen, 5 pounds in the reservoir.

When the pump was shut off from the system that was being evacuated, the pressure dropped very rapidly to 1×10^{-8} mm Hg. To test the effectiveness of the cooled baffle, the refrigerator was turned off for one hour. During this time the pressure rose to 2×10^{-8} mm Hg. The original purpose of the cooled baffle was to reduce the back-diffusion of oil vapor from the MCF-400 pump. Because of the pressure reduction produced by cooling the baffle, it is felt that the baffle will be successful in eliminating oil vapors from the system.

2. Electron Gun

An electron gun for testing in the vacuum system described above has been

47

fabricated in a sealed-off envelope. Siegman (1) has shown, by making an analysis of the region of the potential minimum in front of a space-charge-limited cathode, that a correlation is produced in the electron stream between voltage and current fluctuations. This correlation was produced in the region beyond the potential minimum where only single directional flow occurs. The increase of the correlation value was produced within a few tenths of a volt from the potential minimum. We believe that the value of the correlation can be increased if the electron stream can be made to drift with a velocity that is comparable to its thermal velocity for a greater distance than it drifts when the electron flow is between parallel planes. By causing an increase in the value of the correlation, a reduction in noise figure can be obtained for the amplifier in which the beam is used.

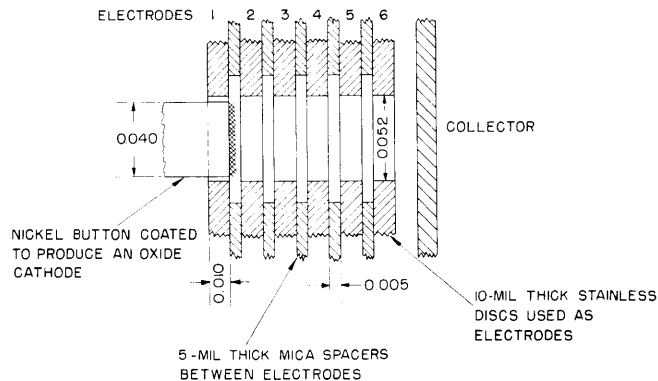The electron gun has a number of closely spaced parallel plates whose potentials

Fig. V-3. Electron gun.

can be varied independently. A cross section showing the significant dimensions is shown in Fig. V-3. A 300-μamp beam can be produced with this structure when the first three electrodes are held at potentials below cathode voltage. The fourth electrode is at +70 volts with respect to the cathode. The beam is produced in an axial magnetic field of 450 gauss.

The electron-gun assembly will be used to supply the electron stream for a low-noise gun, and its usefulness in producing the desired value of correlation will be determined from measurements in the demountable system.

A. Zacharias

References

1. A. E. Siegman, Analysis of multivelocity electron beams by the density-function method, J. Appl. Phys. 28, 1132 (1957).

C. KLYSTRON GAP THEORY

1. Small-Signal Analysis

In the absence of space-charge fields, the interaction of electrons with longitudinal electric fields can be described by a self-consistent theory: (a) The electron motion in an externally applied field is analyzed by using the Lorentz force equation. (b) The reaction of the electron motion upon the applied field is obtained through the conservation-of-energy equation. (c) The analyses of (a) and (b) are connected through the principle of conservation of charge.
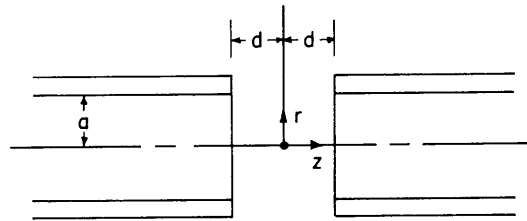

Fig. V-4.   The cylindrically symmetric geometry of a gap.

Consider the cylindrically symmetric geometry of Fig. V-4 (in which there is also symmetry about the z = 0 plane). We assume that the electric field E(z, r) that is present arises from an excitation at the gap only, so that $E(\pm\infty, r) = 0$, and that a gap voltage can be defined as

$$V_g = -\int_{-d}^{d} E(z, a)\, dz \tag{1}$$

For the sake of convenience, we normalize the small-signal complex quantities as follows:

Distance: $\theta = \beta_e z$ with $\beta_e = \dfrac{\omega}{v_o}$

$\rho = \gamma r$ $\gamma = \sqrt{\beta_e^2 - k^2}$

$k = \dfrac{\omega}{c}$

Electric field: $\underline{\underline{E}}(\theta, \rho) = \dfrac{E_z(\theta, \rho)}{\beta_e V_g}$

Kinetic voltage: $\underline{\underline{V}}(\theta, \rho) = \dfrac{V(\theta, \rho)}{V_g}$ Beam current: $\underline{\underline{I}}(\theta, \rho) = \dfrac{I_z(\theta, \rho)}{I_o}$

Gap voltage: $\underline{\underline{V}}_g = \dfrac{V_g}{V_o}$ Gap current: $\underline{\underline{I}}_g = \dfrac{I_g}{I_o}$
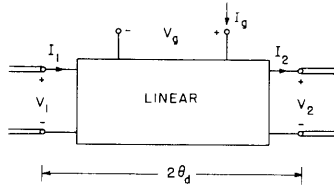
49

Fig. V-5. Linear three-port representation of electron interaction with electric fields of a gap.

where I_O and V_O are, respectively, the time-average current and voltage of the electron stream. The small-signal equations describing the interaction become (θ' is referred to the input of the drift)

$$\underline{V}(\theta, \rho) = e^{-j\theta'} \underline{V}(-\infty, \rho) + e^{-j\theta} \int_{-\infty}^{\theta} \underline{E}(\theta, \rho) e^{j\theta} \, d\theta \tag{2}$$

$$\underline{I}(\theta, \rho) = e^{-j\theta'} \underline{I}(-\infty, \rho) + j \frac{1}{2} \underline{V}_g e^{-j\theta} \int_{-\infty}^{\theta} \underline{V}(\theta, \rho) e^{-j\theta} \, d\theta \tag{3}$$

$$\underline{I}_g = \int_{-\infty}^{\theta} \underline{I}(\theta, \rho) \, \underline{E}(\theta, \rho) \, d\theta \tag{4}$$

The small-signal formalism linearizes the equations and therefore makes the superposition principle applicable. Hence the interaction can be represented by a linear three-port network, as shown in Fig. V-5.

Let

$$V_1 = V(-\infty, \rho) \qquad V_2 = V(\infty, \rho)$$

$$I_1 = I(-\infty, \rho) \qquad I_2 = I(\infty, \rho) \tag{5}$$

then

$$\begin{bmatrix} V_2 \\ I_2 \\ I_g \end{bmatrix} = \begin{bmatrix} y_{11} & 0 & y_{13} \\ Y_{21} & y_{22} & Y_{23} \\ Y_{31} & y_{32} & Y_{33} \end{bmatrix} \begin{bmatrix} V_1 \\ I_1 \\ V_g \end{bmatrix} \tag{6}$$

in which all of the matrix elements can be evaluated by superposition with the aid of Eqs. 2, 3, and 4. It turns out that all of the coefficients in the matrix of Eq. 6 are functions of only two Fourier integrals of the field,

$$\beta = \int_{-\infty}^{\infty} \underline{E}(\theta, \rho) e^{j\theta} \, d\theta \tag{7}$$

50

and

$$\gamma = \int_{-\infty}^{\infty} -j\theta \, \underline{\underline{E}}(\theta, \rho) \, e^{j\theta} \, d\theta \tag{8}$$

If the electric field at the wall, $E(z, a)$, is specified (for example, from a static approximation), then, by the uniqueness theorem, the electromagnetic field everywhere inside the cylinder is determined. The integrals β and γ are then found by Fourier-integral techniques. More importantly, for any given gap, β and γ can be measured by standard perturbation techniques.

As an example, the electronic loading admittance of a gap is

$$Y_{e\ell} = Y_{33} = \frac{I_g}{V_g}\bigg|_{I_1 = V_1 = 0}$$

By using Eqs. 2, 3, 4, and 5 it can be shown that

$$\text{Re}(Y_{e\ell}) = \frac{1}{2} G_o \gamma^* \beta \tag{9}$$

2. Kinetic Power Flow

The interaction of the electron stream with the gap fields will, in general, produce a change in the kinetic power, $\text{Re}[1/2 \, VI^*]$, carried by the electrons. This can readily be obtained from Eqs. 2, 3, 4, 7, and 8. Letting

$$\alpha = \frac{1}{2} G_o (\gamma^* + j\theta_d \beta) e^{-j\theta_d}$$

and

$$P_k = \text{Re}\left[\frac{1}{2} VI^*\right]$$

we find that

$$P_{k2} - P_{k1} = \frac{1}{2} \text{Re}[V_g(\beta I_1)^*] + \frac{1}{2} \text{Re}[V_g(\alpha V_1)^*] + \frac{1}{2}|V_g|^2 \text{Re}(Y_{e\ell}) \tag{10}$$

If the gap is terminated in a passive admittance Y_c,

$$I_g = -Y_c V_g \tag{11}$$

If we let

$$Y = Y_c + Y_{e\ell} \tag{12}$$

then Eq. 10 becomes

51

$$P_{k2} - P_{k1} = -\frac{1}{2} \left| \frac{\alpha\,V_1 + \beta\,I_1}{Y} \right|^2 \text{Re}(Y_c) \tag{13}$$

Equations 10 and 13 are explicit forms of the Chu kinetic power theorem for our small-signal interaction problem.
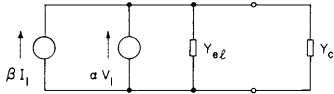

Fig. V-6. The interaction as it appears at the gap circuit terminals.

From Eq. 13 we note that when the interaction is referred to the gap circuit, the equivalent circuit representation is as shown in Fig. V-6. Equation 13 also shows that if the circuit is lossless, the kinetic power in the beam remains unchanged.

A. Bers

D. MULTICAVITY KLYSTRON

The seven-cavity, hollow-beam klystron has been partially assembled for diode tests. A coaxial-to-waveguide transition and vacuum seal have been cold-tested, and a final output-cavity design has been achieved.

1. Preliminary Gun Tests

The hollow-beam gun was assembled, together with the first six cavities (the output cavity and collector were not used). At 50 kv the maximum current was 40 amp, peak (a current density of approximately 8 amps/cm^2) under obviously temperature-limited conditions. The design current is 100 amp (approximately 18 amps/cm^2). Since the first bake-out required 10 days to reach a pressure of 3×10^{-7} mm Hg at 450° C, it is perhaps not surprising that we did not achieve the desired current.

2. Low-Q Output Cavity

The proposed four-loop coupling system for a low-Q output cavity, which was described in the Quarterly Progress Report of January 15, 1958, page 41, did not give the desired results when the separately tested loops were interconnected by a transmission-line system to a single output line. A nonsymmetrical resonant mode whose resonant frequency was in the band that is of interest, was excited in each set of two loops and their respective transmission-line connections. Attempts to shift the resonance far enough away by means of slots in the cavity post were not successful.

We decided to use a two-loop coupling system. Tight coupling was achieved by extending the center conductor of the transmission line to the re-entrant post of the cavity (Fig. V-7). The self-inductance of the loop can be reduced by making the
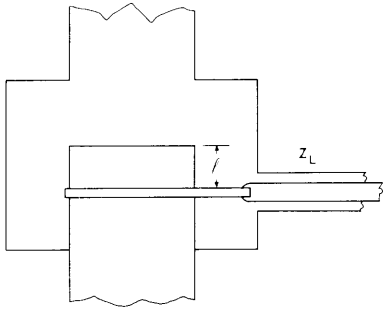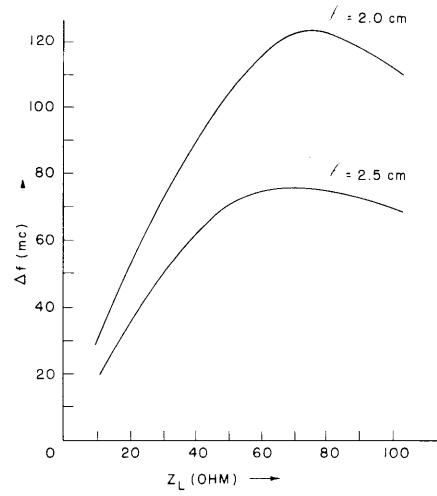
Fig. V-7. Strongly coupled test cavity.

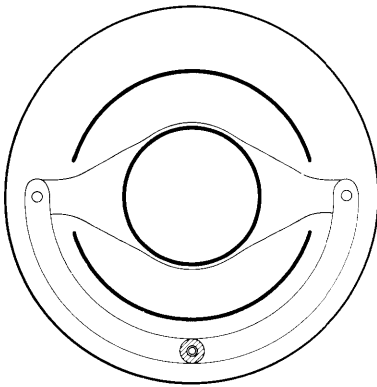Fig. V-8. Bandwidth-load characteristics of strongly coupled cavity.
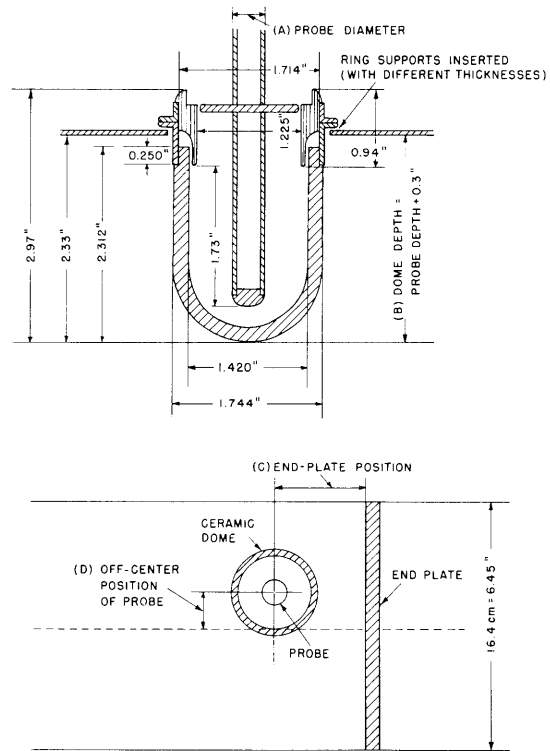

Fig. V-9. Two-loop coupling system.

Fig. V-10. Coaxial-to-waveguide transition with vacuum seal.

53

connection out of a wide strip. In the course of measurements we found that the band-width of the loaded cavity is not a monotonic function of the load impedance.

A re-entrant cavity that is loaded as shown in Fig. V-7 displays a relation between bandwidth Δf and load impedance Z_L, as shown in Fig. V-8. For a given distance ℓ between gap and coupling connection there exists an optimum load impedance for the maximum obtainable bandwidth.

The actual output cavity that was built after these laboratory measurements were made is loaded by two loops (see Fig. V-9). The connections are located 2.2 cm from the gap edge. They are connected to a 60-ohm transmission line. The measured band-width of the loaded cavity was Δf = 160 mc at a center frequency of f_0 = 1260 mc.

The ratio R_s/Q_L of this output structure was measured as 109. In order to find the shunt impedance, different thin-layer resistors were placed across the gap. We assumed that the shunt impedance is equal to that resistor which creates a standing-wave ratio of 1 on the output transmission line. An 860-ohm resistor gave this result.

3. Coaxial-to-Waveguide Transition and Vacuum Seal

A ceramic dome and metal parts for attachment to a coaxial line were furnished by Raytheon Manufacturing Company. The problem was to design the associated rf cir-cuitry to produce a wideband match between the coaxial line ($Z_0 \approx 50$ ohms) and the L-band waveguide. Four parameters could be modified: the diameter and the length of the coaxial inner conductor extending into the dome, the transverse position of the probe on the waveguide, and the position of the waveguide short circuit behind the probe.

The interpretation of the parameters is indicated in Fig. V-10 by the notation A, B, C, and D. The measurements were made with the following parameter variations:

A	0.55"	0.50"	0.45"	0.40"
B	2.33"	2.40"	2.46"	2.525"
C	1.225"	1.35"	1.475"	1.6"
D	0.25"	0.5"	0.75"	1.00"

Variations in dome depth were obtained by inserting ring supports of different thick-nesses between the coaxial line and the waveguide wall, as illustrated in Fig. V-10. Voltage-standing-wave ratios were measured from both the coaxial and waveguide sides of the transition:

a. When measuring from the coaxial side, the waveguide section was terminated in a matched load. The results of the calibration of the matched load are as follows:

Frequency (mc)	1100	1150	1200	1250	1300	1350
VSWR	1.12	1.04	1.07	1.04	1.03	1.02

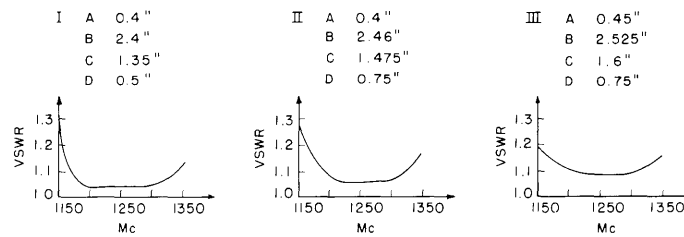| I	A	0.4"	II	A	0.4"	III	A	0.45"
	B	2.4"		B	2.46"		B	2.525"
	C	1.35"		C	1.475"		C	1.6"
	D	0.5"		D	0.75"		D	0.75"

Fig. V-11. Frequency characteristics of coaxial-to-waveguide transition.

b. When measuring from the waveguide side, the coaxial line was terminated in a matched load. The standing-wave ratio was kept below 1.05 between the matched load and transition section at the frequencies that are of interest.

From all the reasonable sets of parameters, the measurements that gave the best results are shown in Fig. V-11.

H. Fock, S. Holly, A. Saharian

E. PLASMA OSCILLATIONS

A study of ion plasma oscillations, in which particular attention was paid to quasi-static propagation in a waveguide loaded with a stationary plasma (1, 2, 3), has been made. The author's Master of Science thesis, entitled "Electron-Stimulated Ion Oscil-ations," will appear as Technical Report 277.

A kinematic study of an ion-oscillation mechanism that is largely an extension of Jepsen's model (4) is included in the technical report. In another paper (5) the dis-persion in a plasma that consists of both stationary ions and an electron beam is inves-tigated on a quasi-static basis; several waves are identified through the use of reasonable approximations.

P. Chorney

References

1. P. Chorney, Theoretical study of electron-stimulated ion oscillations, Quarterly Progress Report, Research Laboratory of Electronics, M.I.T., Oct. 15, 1957, p. 30.

2. P. Chorney, Propagation in a circular waveguide loaded with a nondrifting plasma, Quarterly Progress Report, Research Laboratory of Electronics, M.I.T., Jan. 15, 1958, p. 42.

3. L. D. Smullin and P. Chorney, Properties of ion-filled waveguides, Proc. IRE 46, 360 (1958).

4. R. L. Jepsen, Ion oscillations in electron beam tubes; ion motion and energy trans-fer, Proc. IRE 45, 1069 (1957).

5. L. D. Smullin and P. Chorney, Propagation in ion-loaded waveguides, Proc. Elec-tronic Waveguide Symposium, Polytechnic Institute of Brooklyn (to be published in the Fall of 1958).